



Effect of TiO₂ particle and pore size on DSSC efficiency

V. A. González-Verjan¹ · B. Trujillo-Navarrete¹ · Rosa María Félix-Navarro¹ · J. N. Díaz de León² · J. M. Romo-Herrera² · J. C. Calva-Yáñez³ · J. M. Hernández-Lizalde¹ · E. A. Reynoso-Soto¹

Received: 29 June 2019 / Accepted: 4 June 2020 / Published online: 8 June 2020
© The Author(s) 2020

Abstract

In this work, we report the preparation of TiO₂ nanoparticles with a high surface area, from 120 to 168 m² g⁻¹ by the hydrothermal-microemulsion route and hydrothermal temperature effect over particle size, porosity, and photovoltaic parameter. The TiO₂ samples were characterized by Raman, BET, TEM, SEM-FE, I–V curves, and EIS. The increase of hydrothermal temperature correlates with particle and pore size. Although when the synthesis temperature was 250 °C, the surface area presents an unexpected decrease of c.a. 28%. TiO₂ samples were employed as thin-film photo-anodes for dye-sensitized solar cell (DSSC) solar cells. Photovoltaic results showed that the sample prepared at 250 °C presented the more suitable textural properties for the DSSC application. The prepared TiO₂ materials with a particle size of 6.93 ± 0.59 nm and anatase crystalline phase favor electron transport and diffusion of electrolyte species, which directly impact in solar cell efficiency.

Keywords DSSC · Titanium · Mesoporous · Anatase · Nanoparticles

Introduction

The development of clean alternatives to current power generation is imperative to preserve the global environment. Photovoltaic devices generated electricity directly from sunlight without any emission that could contribute to global warming. Photovoltaic systems are classified based on their components: silicon, semiconductor thin films, organic, polymeric, hybrid, and dye or QD sensitized. A dye-sensitized solar cell (DSSC) is constituted by mesoporous TiO₂ thick film, dye, redox electrolyte, and a counter electrode. Each

component plays a role in electron transport and diffusion [1]. TiO₂ acts as a scaffold to adsorbed dye molecule and transports the electron photogenerated by light absorption and dye regeneration. Several attempts are made to improve TiO₂ transport properties to increase solar energy conversion in DSSC. The morphology, particle, and pore size of TiO₂ play critical roles in photoelectron diffusion and conversion efficiency of DSSC [2]. TiO₂ nanomaterial with different morphologies spherical [3], tubes [4], wire [5], rhombic and squares [6] have been synthesized by various methodologies, differences in morphology promote change in the crystallize size, band-gap energy, and surface area [7]. Materials properties can be modulated by synthesis conditions to decrease the material size, produce different shapes, or increase the surface to volume ration [8]. Since its commercial production TiO₂ has been subjected of extensive research work to improve its properties, many methods are being employed in the synthesis of nano-crystalline TiO₂ with pure phase and specific shape as sol–gel [9], micelle and inverse micelle [10], sol, [11], direct oxidation [12], chemical vapor deposition [13], sonochemical-assisted [14], microwave-assisted [15], and hydrothermal and solvothermal method [16]. Hydrothermal and solvothermal methods present the advantage of simple operation conditions and the ability to produce TiO₂ nanomaterial with different shapes, high surface area, and controlled porosity.

Electronic supplementary material The online version of this article (<https://doi.org/10.1007/s40243-020-00173-7>) contains supplementary material, which is available to authorized users.

✉ E. A. Reynoso-Soto
edgar.alonso@tectijuana.mx

¹ Centro de Graduados E Investigación en Química, Tecnológico Nacional de México, Instituto Tecnológico de Tijuana, Apdo. Postal 1166, 22000 Tijuana, BC, México

² Centro de Nanociencia Y Nanotecnología, Universidad Nacional Autónoma de México, Apdo. Postal 14, 22800 Ensenada, BC, México

³ Centro de Graduados E Investigación en Química, CONACyT-Tecnológico Nacional de México, Instituto Tecnológico Tijuana, Apdo. Postal 1166, 22000 Tijuana, BC, México

In this work, we report a set of experiments to synthesize nano-crystalline TiO_2 with a modulated surface area and porosity to evaluate the effect of being employed as a photo-anode in the DSSC.

Experimental

Materials

Titanium (IV) isopropoxide ($\text{Ti}[\text{OCH}(\text{CH}_3)_2]_4$, 97%), polyethylene glycol *tert*-octylphenyl ether (Triton X100), heptane (C_7H_{16} , 99%), 1-hexanol ($\text{C}_6\text{H}_{14}\text{O}$, 98%), di-tetra-butylammonium-cis-bis(isothiocyanato)bis(2,2'-bipyridyl-4,4'-dicarboxylato) ruthenium (II) ($\text{C}_{58}\text{H}_{86}\text{N}_8\text{O}_8\text{RuS}_2$, 95%), terpineol ($\text{C}_{10}\text{H}_{18}\text{O}$, 95%), 5–15 mPa·s ethyl cellulose (48.0–49.5% w/w ethoxyl basis), 30–70 mPa·s ethyl cellulose (48.0–49.5% w/w ethoxyl basis), acetic acid ($\text{C}_2\text{H}_4\text{O}_2$, 99%), ethanol ($\text{C}_2\text{H}_6\text{O}$, 98%), *tert*-butanol ($\text{C}_4\text{H}_{10}\text{O}$, 99%), 3-methoxypropionitrile ($\text{C}_4\text{H}_7\text{NO}$, 98%), acetonitrile ($\text{C}_2\text{H}_3\text{N}$, 99%), tetra-butylammonium hydroxide ($\text{C}_{16}\text{H}_{36}\text{NOH}$, 98%), tetra-butylammonium iodide ($\text{C}_{16}\text{H}_{36}\text{NI}$, 98%) lithium iodide (LiI, 99%), iodine (I_2 , 99%), and 4-*tert*-butylpyridine ($\text{C}_9\text{H}_{13}\text{N}$, 96%) were obtained from Sigma-Aldrich and use without further purification. All aqueous solutions were prepared with Milli-Q water (18 m Ω). Ti-Nanoxide T/SP, Platisol T/SP as platinum precursor for photo-cathode, and 25 μm thermoplastic and conductive glass TCO30-8 with 8 Ω/sq were acquired from Solaronix.

Synthesis of mesoporous TiO_2 particles

Mesoporous TiO_2 was prepared according to the procedure reported by Xiangcun with slight modifications [17]. Typically, in a Teflon-line autoclave of 125 mL were added 0.97 mL of heptane and 0.33 mL of hexane with 0.015 mol of TritonX-100 mixing with 0.48 mol of H_2O and stirred for some minutes. Then, 1 mL of titanium isopropoxide was added for every 10 mL of the reaction mixture. Subsequently, the reaction mixture was put into an oven for hydrothermal treatment at a different temperature from 120 to 250 $^\circ\text{C}$ for 13 h. After that, the autoclave was cooled down naturally to room temperature, and then, the white solid was filtered under vacuum pressure and washed with water and ethanol several times before drying in air at 100 $^\circ\text{C}$. After drying, the solid was thermally treated at 200 $^\circ\text{C}$ to remove organic compounds.

Characterization of synthesized materials

Several techniques were used in the characterization of mesoporous TiO_2 ; Raman spectra were recorded on a DXR 2 Smart Raman spectrometer (Thermo Scientific)

equipped with a diode laser of 738 nm wavelength. N_2 adsorption–desorption isotherms determined the textural properties of the materials at -196 $^\circ\text{C}$ on a TriStar II 2020 Micromeritics equipment. Before the experiments, the materials were degassed at 125 $^\circ\text{C}$ in vacuum for 5 h. The volume of the adsorbed N_2 was normalized to the standard temperature and pressure. Specific surface area (S_{BET}) was calculated by the Brunauer–Emmet–Teller (BET) equation applied to the range of relative pressures $0.1 < P/P_0 < 0.3$. The average pore diameter (P_d) was calculated by applying the Barret–Joyner–Halenda method (BJH) to the adsorption branches of the N_2 isotherms. The total pore volume (P_v) was obtained from the saturation point ($P/P_0 \sim 0.99$).

TEM micrographs were obtained from a JEOL JEM-2010 (200 kV of accelerating voltage) instrument to determine the morphology and particle size. The sample was ultrasonically dispersed in ethanol, and a drop was placed on a copper grid coated with a holey carbon film.

SEM micrographs have been acquired in a JEOL JSM-7800F Schottky FE-SEM instrument to evaluate the mesoporosity of the TiO_2 sample, using accelerating voltage a 3.0 kV.

The photovoltaic measurements and electrochemical impedance spectroscopy under illumination were done using a light source AM 1.5 solar simulator ABB (Oriol LCS-100) coupled with a potentiostat/galvanostat (Bio-Logic VMP-300). The incident light intensity was 100 mW cm^{-2} calibrated with a standard Si solar cell.

Dye-sensitized solar cell fabrication

The photo-anode and cathode were prepared using fluorine-doped tin oxide (FTO)-coated glass slides of 8 Ω/sq (Solaronix TCO30-8). For cathodes, a 1 mm-diameter holes were drilled to introduce the electrolyte. Before solar cell fabrication, FTO glass slides were cleaned by sonication with a detergent solution and deionized water, and rinsed with Milli-Q water and ethanol, followed by H_2O_2 at 1% treatment under UV light. At first, the cleaned FTO glass slides were treated with 40 mM TiCl_4 aqueous solution at 70 $^\circ\text{C}$ for 40 min and then rinsed with water and ethanol [18]. The preparation of TiO_2 pastes was carried out as reported by Gratzel et al. [19]; 0.006 mol of TiO_2 was mixed with acetic acid in a mortar for 5 min, following the addition of H_2O and ethanol; after that were added 0.012 mol of terpineol mixed in the mortar and added to an ethanolic solution of ethyl cellulose at 20%. Finally, ethanol was evaporated to obtain the corresponding TiO_2 paste.

The active layer (i.e., the photo-anodes) was deposited by the doctor blade method with an active area of 0.2 cm^2 . TiO_2 pastes were coated onto the TiCl_4 pre-treated FTO glass slides and thermally annealed at 375 $^\circ\text{C}$ for 5 min, 450 $^\circ\text{C}$ for 15 min, and 500 $^\circ\text{C}$ for 15 min. After that, the

photo-anodes were treated a second time with 40 mM TiCl_4 aqueous solution at 70 °C for 30 min and then rinsed with distilled water and ethanol. Finally, thermal treatment of 450 °C for 30 min was applied to photo-anodes. After thermal treatment, when the temperature cooled to about 100 °C, the photo-anodes were sensitized immersing in the N719 dye solution in acetonitrile/tert-butanol mixture (50:50) at $3 \times 10^{-4} \text{ mol L}^{-1}$ for 24 h; the dye excess was rinsed with ethanol.

The counter electrodes were prepared with a Pt catalyzer (T/SP SOLARONIX) using the doctor blade method, and then treated at 500 °C for 30 min. The anode and counter electrode were then sealed together using a 25 μm thermoplastic (SOLARONIX DuPont Surlyn®). The cell was filled with I^-/I_3^- redox couple. The redox electrolyte was constituted by I_2 0.05 mol L^{-1} , LI 0.1 mol L^{-1} , 4-tert-butylpyridine 0.5 mol L^{-1} , and tetra-butylammonium iodide 0.6 mol L^{-1} in a mixture of acetonitrile and 3-methoxypropionitrile (50:50).

N719 dye charge analysis

Dye desorption was accomplished by immersing the dye-sensitized TiO_2 anodes into 0.1 M TBAOH (tetra-butylammonium hydroxide) in ethanol for 24 h and then rinsing for 10 to 20 min with ethanol, and measured by UV–Vis spectroscopy.

Results and discussion

Raman spectroscopy

Raman spectra of TiO_2 samples synthesized at different temperatures are given in Fig. 1. The spectra of all samples show the bands that are assigned to Raman active mode of the anatase crystal; typically, TiO_2 bands are reported at 144 (E_g), 197 (E_g), 399 (B_{1g}), 519 (B_{1g}), and 639 cm^{-1} (E_g) [20]. In our case, temperature variation shows a shift to higher Raman frequencies and decrease the intensity of all bands, as shown in Fig. 1, the results of displacement and full width at half maximum (FWHM) are resumed in Table 1. This change in the shape, intensity, or displacement of Raman bands is attributed to change in crystal dimensions (i.e., a behavior according to the phonon confinement model), pressure effect on the grains, or surface tension producing a high frequency [21].

Textural characterization

Textural properties of the nanomaterial are a measure of available space, or total volume that would be occupied by molecules in reactions and mass transfer processes in the specific case of the DSSC dyes could occupy this space.

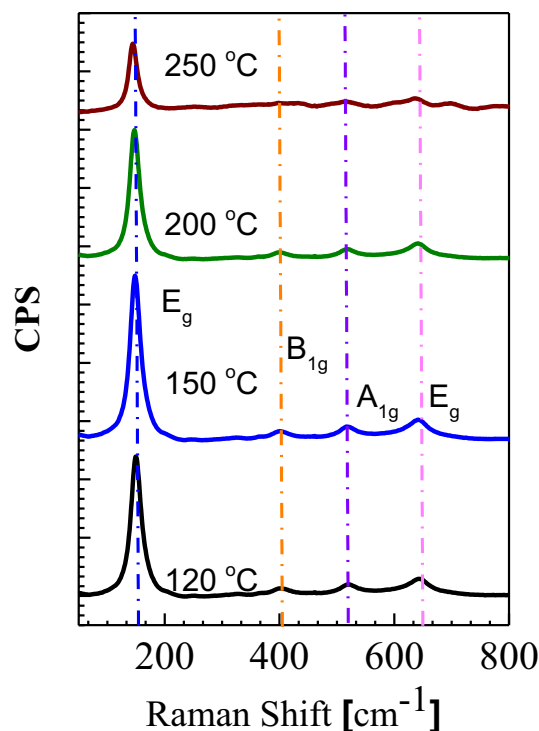


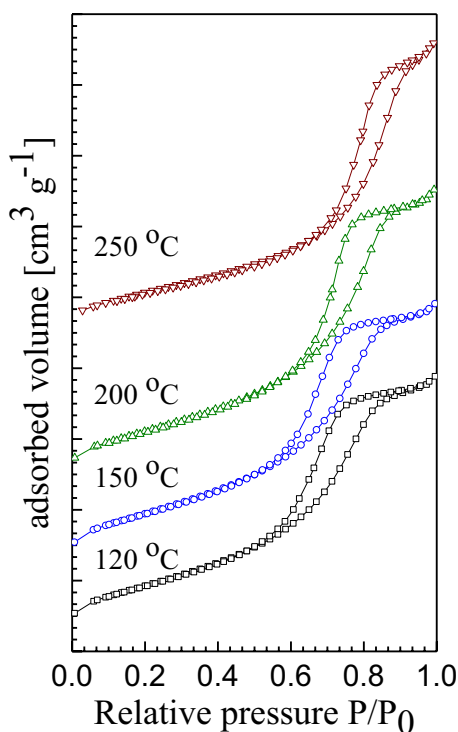
Fig. 1 Raman spectra of mesoporous titanium oxide samples

Nitrogen adsorption/desorption isotherms of mesoporous TiO_2 samples synthesized at varying hydrothermal temperature are provided in Fig. 2.

Adsorption–desorption isotherms type IV resulted in all materials; this type is characteristic of materials with mesoporosity and high molecular adsorption energy. As we can observe in Table 2, the total surface area for samples seems to be the same as the general trend within the uncertainty of the technique ($\pm 6 \text{ m}^2 \text{ g}^{-1}$). Nevertheless, the sample calcined at the highest temperature (250 °C) presented a contraction c.a. 32%. Samples prepared at 120 °C, 150 °C, 200 °C, and 250 °C showed H1 hysteresis loops displaying nearly vertical and parallel adsorption and desorption branches, and this behavior could be related to the arrangement of cavities between spherical particles or to well-defined cylindrical pores [22]. Differences are more likely observed in the total pore volume (P_v), in the average pore size (D_{BJH}) or the pore size distribution plots. In this case, the P_v seems to be constant for all samples. However, the D_{BJH} presented the most significant value among series (provided as supplementary information) due to a general increase in the size of mesopores. These results suggested us that the material's textural properties are suitable for the intended use of this work (photo-anodes in DSSC). As we can observe in Table 2, from the sample synthesized at 150 °C, the decay in surface area is accompanied by a rise in the average pore size

Table 1 Raman displacements of mesoporous TiO₂ samples

Sample	Raman E_g Shift (cm ⁻¹)	FWHM E_g (cm ⁻¹)	Raman B_{1g} shift (cm ⁻¹)	FWHM B_{1g} (cm ⁻¹)	Raman B_{1g} Sshift (cm ⁻¹)	FWHM B_{1g} (cm ⁻¹)	Raman B_{1g} shift (cm ⁻¹)	FWHM B_{1g} (cm ⁻¹)
TiO ₂ -120	150.04	22.85	401.48	30.03	521.19	38.96	643.28	36.56
TiO ₂ -150	148.24	22.64	400.00	33.79	517.27	27.72	641.89	54.05
TiO ₂ -200	146.94	20.69	399.15	34.36	518.37	33.27	641.23	46.28
TiO ₂ -250	144.68	18.44	ND	ND	ND	ND	ND	D

**Fig. 2** N₂ adsorption–desorption spectra of mesoporous TiO₂ samples**Table 2** Textural properties of TiO₂ samples from N₂ adsorption/desorption analysis

Sample*	S_{BET} (m ² g ⁻¹)	P_v $V_{P/P_0=0.95}$ (cm ³ g ⁻¹)	D_{BJH} (Å)
TiO ₂ -120	167	0.29	57.83
TiO ₂ -150	170	0.29	57.51
TiO ₂ -200	164	0.32	64.70
TiO ₂ -250	125	0.30	81.22

*All samples were thermally treated at 200 °C for 3 h

(D_{BJH}), this is due to the increase in the nanoparticle size as a function of synthesis conditions (i.e., temperature and pressure inside the vessel), in which arrangement, an

increment in diameter involves larger space of the cavities that form between them, and a higher mass contained in each particle.

Electron microscopy TEM and FE-SEM

Once the crystalline phase and porosity of the TiO₂ samples prepared by the hydrothermal method were identified, the morphology was investigated by TEM (Fig. 3). The morphology of mesoporous TiO₂ samples calcinated at 200 °C has a spherical and semi-spherical shape, as can be shown in the high magnification image (supplementary material). The particle-size distribution is $\mu = 4.42 \pm 0.53$ nm, $\mu = 5.29 \pm 0.79$ nm, $\mu = 5.42 \pm 1.27$, and $\mu = 6.93 \pm 0.59$ nm, for TiO₂ samples prepared at 120, 150, 200, and 250 °C respectively. These results suggest that mesoporosity is due to the interconnection of particles, and Triton X100 molecules stabilize this during microemulsion synthesis. However, when temperature increase during hydrothermal treatment, the microemulsion system becomes unstable or more flexible, increasing the micelle exchange promoting a particle-size increment as reported by Xiangcu et al. [17].

It can be seen, the FE-SEM images in Fig. 4, the material shape structure, and possibly the porosity are the result of the TiO₂ nano-crystalline particle aggregation when the thermal treatment removed surfactant Triton X100 molecules. These particles present homogenous spherical form, and the aggregate becomes visible particles with mentioned porosity. Also was carried out the analysis of photo-anodes thermally treated by FE-SEM, the image (supplementary material) does not show any modification in the material shape structure or aggregates that generate the porosity of the material.

Current–voltage measurement

The photocurrent density–voltage curves of DSSC fabricated with the TiO₂ samples are shown in Fig. 5, with the detailed photovoltaic parameter listed in Table 3. The highest efficiency was achieved by the cell fabricated was with the sample TiO₂ at 150 °C, with open-circuit voltage (V_{oc}) of 729 mV, short circuit current density (J_{sc}) of

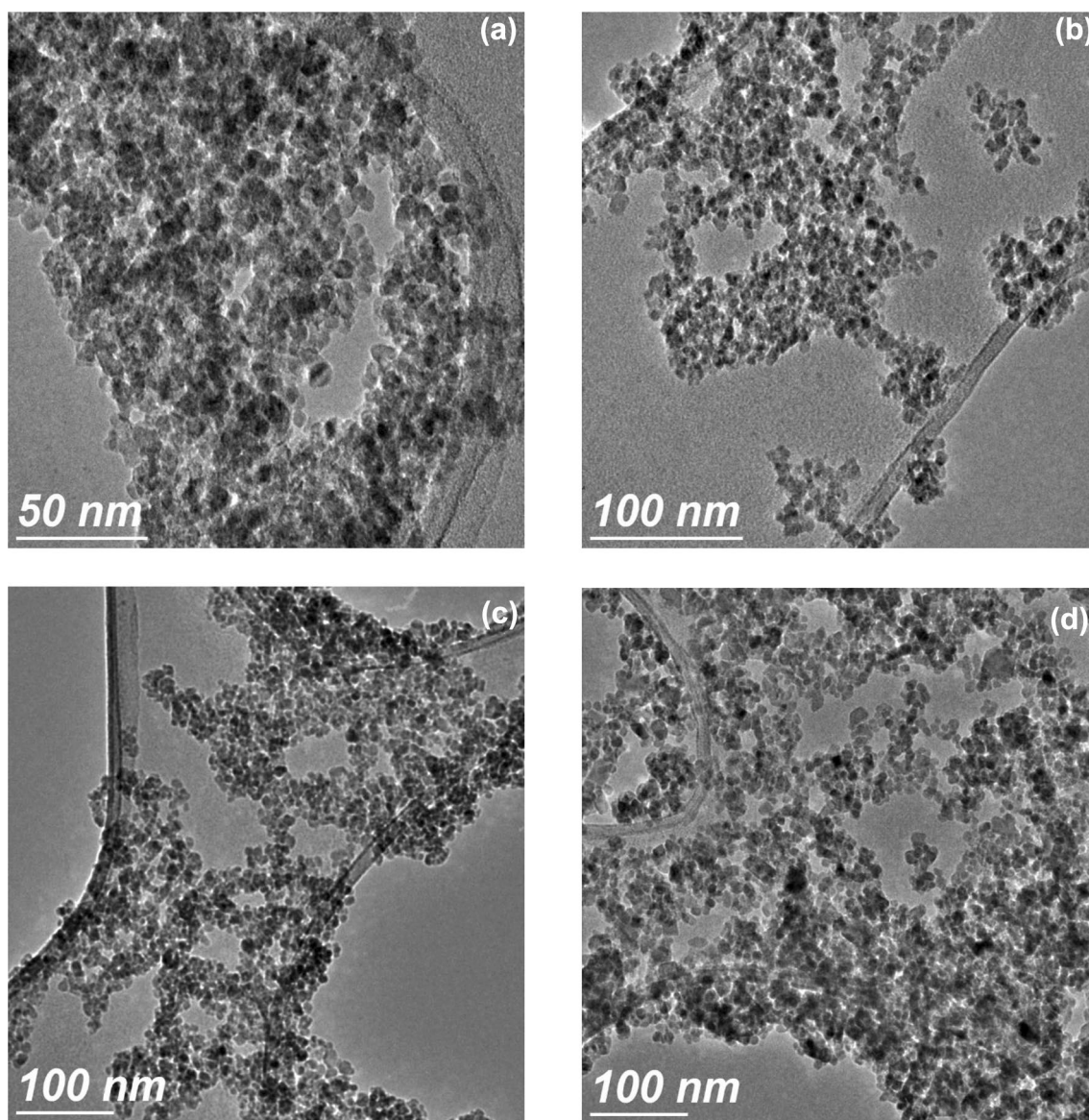


Fig. 3 TEM image of TiO₂ samples prepared by hydrothermal at **a** 120 °C, **b** 150 °C, **c** 200 °C, and **d** 250 °C

18.59 mA cm⁻², fill factor (FF) of 47.4%, dye loading of 1.91×10^{-6} mol cm⁻², and energy conversion efficiency (η) of 6.43%. The samples with average pore size around 5.7–6.5 nm present similar dye loading approximately 1.7 to 1.9×10^{-6} mol cm⁻²; this similarity between the samples is attributed to the surface area ($160 \text{ m}^2 \text{ g}^{-1}$). The solar cell assembled with the sample prepared at 250 °C that reaches dye adsorption of only 0.67×10^{-5} mol cm⁻² shows an energy conversion efficiency of 5.76% with FF of 61.5%. This behavior may be due to multiple factors such as low charge-transfer resistance at the counter electrode, an improvement of electron transport on TiO₂ mesoporous film, and better diffusion of electrolyte species due to all larger pore and particle size of TiO₂-250 compared with

TiO₂-150 sample, consistent with reports by Cheng et al. [23].

Electrochemical impedance spectroscopy of dye-sensitized solar cell

To elucidate the charge-transfer kinetics on the DSSC based on TiO₂ mesoporous samples, electrochemical impedance spectroscopy (EIS) was employed. Within the frequency range analyzed by EIS (100 kHz–1 Hz), three-time constants are represented by two distinct semicircles in the complex plane plot (Fig. 6). To decrease the frequency, the first semicircle is related to the charge to the charge-transfer processes at Pt/electrolyte interface (ω_{CE}), and the second corresponds

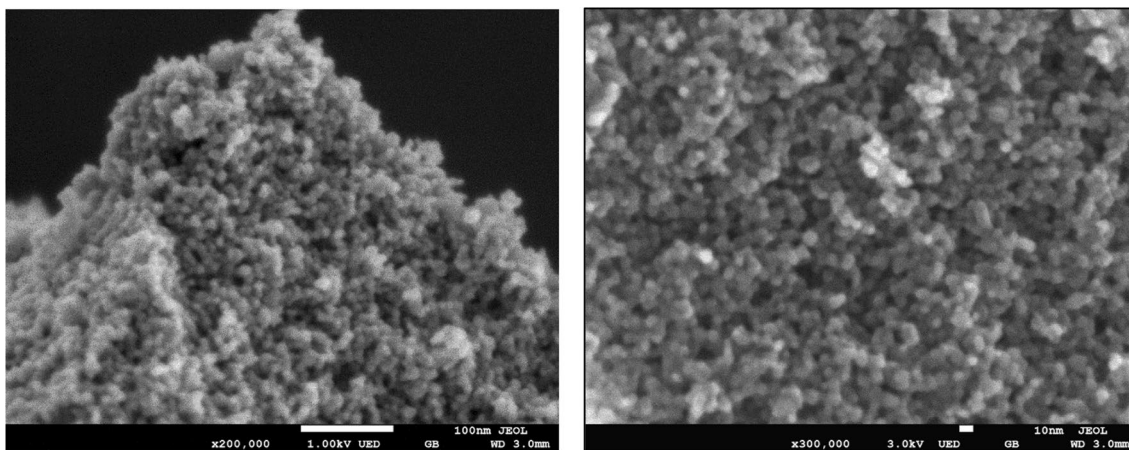


Fig. 4 FE-SEM image of TiO₂ sample synthesized at 150 °C and thermally treated at 200 °C

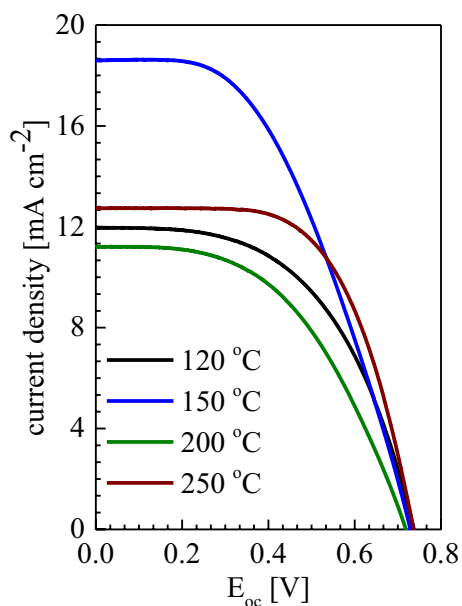


Fig. 5 *J-V* measurement of dye-sensitized solar cells with mesoporous TiO₂ samples

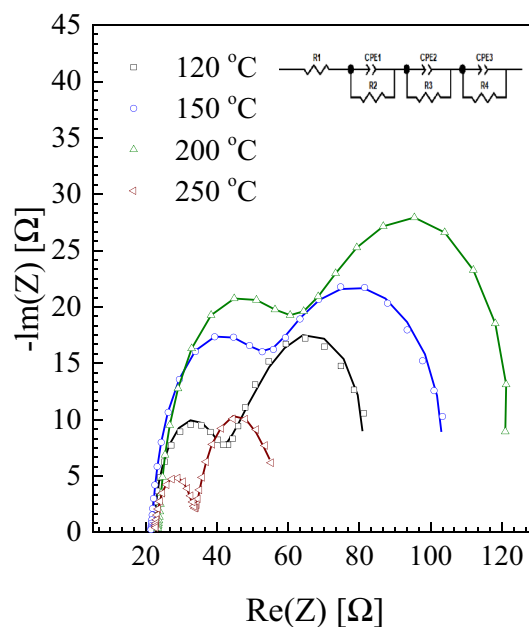


Fig. 6 EIS analysis of dye-sensitized solar cells with mesoporous TiO₂ samples

Table 3 Photovoltaic parameters of DSSC fabricated with the TiO₂ samples

Sample	<i>J</i> _{sc} (mA cm ⁻²)	oc (mV)	<i>η</i> (%)	FF	Dye loading (× 10 ⁻⁶ mol cm ⁻²)
TiO ₂ -120	11.96	737	4.72	53.5	1.91
TiO ₂ -150	18.59	729	6.43	47.4	1.91
TiO ₂ -200	11.20	719	4.02	49.9	1.74
TiO ₂ -250	12.73	736	5.76	61.5	0.67

to the electron diffusion in the TiO₂ mesoporous film and electron back reaction with oxidized redox species at the TiO₂/electrolyte interface, the time constant for electron transport diffusion appears at the high-frequency region of the second semicircle (ω_d), while the peak frequency of that semicircle corresponds to the electron back reaction (ω_k), [24]. Nyquist complex plane pots were fitted using EC-Lab[®] software, and obtained parameters are presented in Table 4.

Based on the parameters obtained from the adjustment of the Nyquist plots, it is possible to observe a significant variation in the charge-transfer resistance in the Pt/electrolyte interface (*R*₂), due to the non-homogeneity between the

Table 4 EIS parameters of the dye-sensitized solar cells with mesoporous TiO₂ samples

Sample	R_2 (Ω)	R_3 (Ω)	k_{eff} (s^{-1})	τ_{eff} (s)	$C_{\mu 3}$ (mF cm^{-2})
TiO ₂ -120	20.19	45.01	1.009	0.991	5.37
TiO ₂ -150	29.32	59.46	31.62	0.031	3.62
TiO ₂ -200	40.27	65.64	21.55	0.046	2.47
TiO ₂ -250	11.13	24.24	6.81	.147	7.82

counter electrodes used in the analyzed DSSCs. The variation in this resistance is reflected in an increase of series resistance in cells and, consequently, a variation in the fill factor for each cell, it is then observed that the cell based on the TiO₂-250 sample has the lowest R_2 (11.13 Ω) and present the best FF (61.5) compared to the TiO₂-200 sample with R_2 (40.27 Ω) and FF (49.9). From the second semicircle of the complex plane analysis, the value of the sum of electron transport resistance in TiO₂ (R_w) and charge-transfer resistance related to recombination of the electron (R_k) at the TiO₂/electrolyte interface (R_3), chemical capacitance ($C_{\mu 3}$), the effective rate constant for recombination (k_{eff}), and effective lifetime of electrons (τ_{eff}) were calculated; again the TiO₂-250 sample has the lowest R_3 (24.24 Ω), τ_{eff} of 0.147 s, and the highest C_{μ} (7.82 mF cm^{-2}), indicating a lower ability to release the electrons that are confined into the TiO₂ conduction band, decreasing the efficiency in the charge transport through the mesoscopic film and reducing the DSSC efficiency. The chemical capacitance ($C_{\mu 3}$) measured in DSSC is related only to the variation of the electron chemical potential in TiO₂ electrode, and reflects the capability of a system to accept or release additional carriers by the change of electron concentration in the TiO₂ conduction band with respect to thermal equilibrium [25]. On the other hand, the TiO₂-150 sample has a high R_3 , the lowest τ_{eff} and low C_{μ} value, (0.031 s and 3.62 mF cm^{-2} , respectively), which means a better charge collection in the photoanode and, consequently, the best η (6.43%). For all samples, the shape of the semicircle indicates that R_w is much greater than R_w ; therefore, a high value of R_3 also means low recombination and better transport of the charge carriers [26]. A compelling case is the TiO₂-200 sample which has the highest R_3 value, low τ_{eff} and the lowest C_{μ} value (0.046 s and 2.37 mF cm^{-2} respectively), which would represent a good charge transport through the photoelectrode; however, the high value of R_2 limits the process of reduction of the oxidized species in the electrolyte, this reduces the amount the species responsible for extracting holes from the photo-anode generating more substantial recombination and, therefore, the lowest η (4.02%). Then, we can affirm that the efficiency of a DSSC depends on the sum of multiple factors such as the low resistance to the charge transfer in the

counter electrode, the low useful lifetime of the electron, and the functional capacity of TiO₂ to release the photogenerated electrons.

Conclusion

Mesoporous TiO₂ nanoparticles with controlled pore size and high surface area were successfully synthesized using the Triton X100 surfactant and hydrothermal method varying synthesis temperature. Results indicated that pore size modulation improve electrolyte species diffusion around TiO₂ film and the decrease of surface area reduces electron transit time through the film, increasing the number of trapping sites which promotes high photocurrent and efficiency of the solar cell by a better electron transport as Helmholtz capacitance shows.

Acknowledgements The authors thank Tijuana Technological Institute for providing the facilities for this research. V. A. González-Verjan wishes to thank CONACyT for the masters' scholarship. Also, the authors thank CONACyT, TecNM, and PRODEP for the financial assistance through the projects PN-2015-92, 272894, 175925, 5273.19-P, 5625.15-P, and ITTIJ-PTC-009 respectively. We are thankful to Francisco Ruiz, Israel Gradilla, Eloisa Aparicio, and Jaime Mendoza for technical assistance.

Open Access This article is licensed under a Creative Commons Attribution 4.0 International License, which permits use, sharing, adaptation, distribution and reproduction in any medium or format, as long as you give appropriate credit to the original author(s) and the source, provide a link to the Creative Commons licence, and indicate if changes were made. The images or other third party material in this article are included in the article's Creative Commons licence, unless indicated otherwise in a credit line to the material. If material is not included in the article's Creative Commons licence and your intended use is not permitted by statutory regulation or exceeds the permitted use, you will need to obtain permission directly from the copyright holder. To view a copy of this licence, visit <http://creativecommons.org/licenses/by/4.0/>.

References

1. Lee, C.-R., Kim, H.-S., Park, N.-G.: Dependence of porosity, charge recombination kinetics and photovoltaic performance on annealing condition of TiO₂ films. *Front. Optoelectron. China*. **4**, 59–64 (2011)
2. Zhao, D., Peng, T., Lu, L., Cai, P., Jiang, P., Bian, Z.: Effect of annealing temperature on the photoelectrochemical properties of dye-sensitized solar cells made with mesoporous TiO₂ nanoparticles. *J. Phys. Chem. C*. **112**, 8486–8494 (2008)
3. Chau-Kuang, L.-L., Wei-Wen, D.: Process optimization of preparing spherical titania colloids with uniform distribution using artificial neural networks. *Colloids Surf. A Physicochem. Eng. Aspects*. **320**, 68–73 (2008)
4. Nakata, K., Liu, B., Ishikawa, Y., Sakai, M., Saito, H., Ochiai, T., Sakai, H., Murakami, T., Abe, M., Takagi, K., Fujishima, A.: Fabrication and photocatalytic properties of TiO₂ nanotube arrays modified with phosphate. *Chem. Lett*. **40**, 1107–1109 (2011)

5. Suárez, F.-J., Sevilla, M., Álvarez, S., Valdés, T., Fuerte, A.-B.: Synthesis of highly uniform mesoporous sub-micrometric capsules of silicon oxycarbide and silica. *Chem. Mater.* **19**, 3096–3098 (2007)
6. Calatayud, D.-G., Rodríguez, M., Jardiel, T.: Controlling the morphology of TiO₂ nanocrystals with different capping agents. *Bol. Esp. Cer. Vid.* **54**, 159–165 (2015)
7. Zhang, H., Zhang, H., Zhu, P., Huang, F.: Morphological effect in photocatalytic degradation of direct blue over mesoporous TiO₂ catalysts. *ChemistrySelect.* **2**, 3282–3288 (2017)
8. Alivisatos, A.-P.: Perspectives on the physical chemistry of semiconductor nanocrystals. *J. Phys. Chem.* **100**, 13226–13239 (1996)
9. Pierre, A.-C., Pajonk, G.-M.: Chemistry of aerogels and their applications. *Chem. Rev.* **102**, 4243–4266 (2002)
10. Hong, S.-S., Lee, M.-S., Park, S.-S., Lee, G.-D.: Synthesis of nanosized TiO₂/SiO₂ particles in the microemulsion and their photocatalytic activity on the decomposition of *p*-nitrophenol. *Catal. Today.* **87**, 99–105 (2003)
11. Niederberger, M., Bartl, M.-H., Stucky, G.-D.: Benzyl alcohol and titanium tetrachloride a versatile reaction system for the nonaqueous and low-temperature preparation of crystalline and luminescent titania nanoparticles. *Chem. Mater.* **14**, 4364 (2002)
12. Wu, J.-M.: Low-temperature preparation of titania nanorods through direct oxidation of titanium with hydrogen peroxide. *J. Cryst. Growth.* **269**, 347–355 (2004)
13. Pradhan, S.-K., Reucroft, P.-J., Yang, F., Dozier, A.: Growth of TiO₂ nanorods by metalorganic chemical vapor deposition. *J. Cryst. Growth.* **256**, 83–88 (2003)
14. Blesic, M.-D., Saponjic, Z.-V., Nedeljkovic, J.-M., Uskokovic, D.-P.: TiO₂ films prepared by ultrasonic spray pyrolysis of nano-size precursor. *Mater. Lett.* **54**, 298–302 (2002)
15. Corradi, A.-B., Bondioli, F., Foche, B., Ferrari, A.-M., Grippo, C., Mariani, E., Villa, C.: Conventional and Microwave-Hydrothermal Synthesis of TiO₂ Nanopowders. *J. Am. Ceram. Soc.* **88**, 2639 (2005)
16. Li, X.-L., Peng, Q., Yi, J.-X., Wang, X., Li, Y.-D.: Near monodisperse TiO₂ nanoparticles and nanorods. *Chem. Eur. J.* **12**, 2383 (2006)
17. Xiangcun, L., Wenji, Z., Gaohong, H.: Morphology control of TiO₂ Nanoparticle in microemulsion and its photocatalytic property. *ACS Sustain. Chem. Eng.* **2**, 288–295 (2014)
18. Ito, S., Murakami, T.-N., Comte, P., Liska, P., Grätzel, C., Nazeeruddin, M.-K.: Grätzel, M.: Fabrication of thin film dye sensitized solar cells with solar to electric power conversion efficiency over 10%. *Thin Solid Films* **516**, 4613–4619 (2008)
19. Ito, S., Chen, P., Comte, P., Nazeeruddin, M.-K., Liska, P., Péchy, P., Grätzel, M.: Fabrication of screen-printing pastes from TiO₂ powders for dye-sensitized solar cells. *Prog. Photovolt. Res. Appl.* **15**, 603–612 (2007)
20. Arsov, L.-D., Kormann, C., Plieth, W.: Electrochemical synthesis and in situ Raman spectroscopy of thin films of titanium dioxide. *J. Raman Spectrosc.* **22**, 573 (1991)
21. Zhang, W.-F., He, Y.-L., Zhang, M.-S., Yin, Z., Chen, Q.: Raman scattering study on anatase TiO₂ nanocrystals. *J. Phys. D Appl. Phys.* **33**, 912–916 (2000)
22. Keshavarzi, R., Mirkhani, V., Moghadam, M., Tangestaninejad, S.: Mohammadpoor, I.: Performance Enhancement of Dye-Sensitized Solar Cells Based on TiO₂ Thick Mesoporous Photoanodes by Morphological Manipulation. *Langmuir* **31**, 11659–11670 (2015)
23. Chen, Y., Huang, F., Xiang, W., Chen, D., Cao, L., Spiccia, L., Caruso, R.-A., Cheng, Y.-B.: Effect of TiO₂ microbead pore size on the performance of DSSCs with a cobalt based electrolyte. *Nanoscale* **6**, 13787–13794 (2014)
24. Sarker, S., Saleh, A., Seo, H.: Electrochemical impedance spectra of dye-sensitized solar cells: fundamentals and spreadsheet calculation. *Int. J. Photoenergy* **2014**, 1–17 (2014)
25. Bisquert, J.: Chemical capacitance of nanostructured semiconductors: its origin and significance for nanocomposite solar cells. *Phys. Chem. Chem. Phys.* **5**, 5360–5364 (2003)
26. Adachi, M., Sakamoto, M., Jiu, J., Ogata, Y., Isoda, S.: Determination of parameters of electron transport in dye-sensitized solar cells using electrochemical impedance spectroscopy. *J. Phys. Chem. B* **110**, 13872–13880 (2006)

Publisher's Note Springer Nature remains neutral with regard to jurisdictional claims in published maps and institutional affiliations.